ELECTRON TRANSPORT AND SECONDARY EMISSION IN A SURFACE OF SOLAR CELL

P. Degond, R. Talaalout, M.-H. Vignal
MIP, UMR CNRS 5640

Université P. Sabatier	INSA
118, route de Narbonne	Complexe scient. de Rangueil
31062 Toulouse cedex 4	31077 Toulouse cedex 4

Abstract— **We study the primary discharge of a solar cell involving secondary emission and desorption. By establishing a fluid model, numerical simulation are performed leading to qualitative informations with regard to the plasma generated by the discharge.**

I. Introduction

Future solar arrays are being designed for much higher voltage operations in order to meet high power demands. During the use of high voltage solar arrays, discharges mostly occur on the surface of the solar cells. According to recent publications, the trigger of electric arcs involves the creation of a primary discharge where electron secondary emission plays an important role.

A schematic of a conventional solar cell is shown in figure 1.

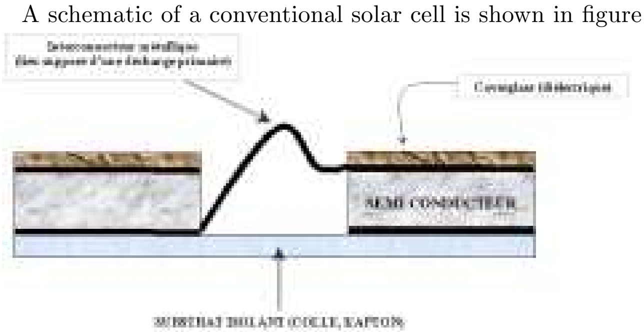

Figure 1 : Conventional solar cell

In a recent work, M.Cho and D.E.Hasting (refs. 4,5) studied the mechanism of secondary arcs formation. They suggested that a neutral gas is desorbed from the side surface of the coverglass by electron bombardement, a phenomenon known as Electron Stimulated Desorption (ESD). The bombarding electrons are emitted from the interconnector, as observed experimentally and determined by Snyder et al (ref 11) and also from the coverglass as a result secondary electron emission. Then the desorbed neutrals accumulate in the gap between the coverglass and the interconnector forming a high pressure gas layer which can breakdown because of the electron current flowing through it.

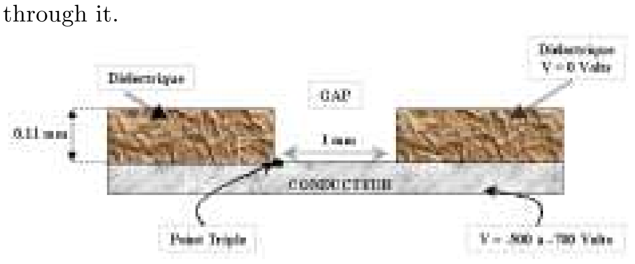

Figure 2

The model studied by M.Cho and D.E.Hasting (Refs 4,5) is shown on figure 2.It consists in dielectric materials placed on a negatively biased conductor in a plasma environment. For a solar array, the dielectrics materials corresponds to the coverglass and adhesives and the conductor corresponds to the interconnector. The solar cell itself is considered lumped with the interconnector.

In this configuration Cho and Hasting (Refs. 4,5) studied the charging of the dielectric materials. They proposed a numerical model for the mechanism of the electric arc formation. The simulation, which are based on particle methods, are stopped when the plasma density becomes too large.

The purpose of this paper is to study the primary discharge and the generated plasma by establishing a fluid model leading to a more macroscopic description than the model given by (Refs. 4,5) and then, enabling numerical simulations at a lower cost. According to M.Cho and D.E.Hasting (Refs 4,5) we suppose that the primary discharge is due to a combination of enhanced field emission at certain sites (particularly, the triple point where metallic parts, dielectrics and vacuum meet), electron secondary emission and electron stimulated desorption of the neutral gas adsorbed on the surface. The important terminologies we use regarding to the region of interest are *dielectric side surface*, the surface perpendicular to the conductor surface; *dielectric front surface*, the surface parrallel to the conductor; *the triple point* where the conductor, the dielectric and the vacuum meet; and *interconnector region*, the region near the triple junction where the electric field is strong (see figure 3).

Figure 3

II. Mathematical modelling

From a kinetic model, P. Degond (Ref. 6) has derived a diffusion model describing the motion of charged particles in a surface potential subject to collisions with a solid surface. In this configuration the electrons emitted from the metallic parts are confined along the dielectric surface and undergo many collisions with the surface (see [12] for more details and references). We consider that particles emitted from the triple point are subject to a longitudinal potential $\Phi_0(x)$ which transports them along the dielectric surface. In a same time, particles are attracted back to the surface by a transverse potential $\Psi(z)$. Particles colliding with the surface suffer a large number of physical process, like attachment to the side surface and secondary emission. For the rigorous derivation of the model, the interaction of the electrons with the side surface should be neerly elastic. In pratice, this is not really the case but the model still leads to satisfactory results (see [12] for more details and references). The resulting macroscopic dynamics of the electrons along the surface is a diffusion process in an extended space consisting of the position and the energy coordinates of the electrons. It consists of a diffusion equation for the distribution function $F(x,\varepsilon)$. The quantity $N(\varepsilon)F(\varepsilon)\,dx d\varepsilon$ is the number of particles in a volume, $dxd\varepsilon$ near the point (x,ε). $N(\varepsilon)$ is the 'density of state' (see Ref. 6) and is given by

$$N(\varepsilon) = \frac{8\sqrt{2}\pi}{3}\frac{1}{q\,|E_t|}\frac{\varepsilon^{3/2}}{m^{3/2}} \tag{1}$$

in the case of a linear transverse potential profile

$$\Psi(z) = -E_T.z. \tag{2}$$

where E_T is the electric field in the perpendicular direction to the dielectric side surface.

A. *The energy transport model*

A.1 Derivation of the energy transport model

The model derived in (Ref. 6) gives access to the energy distribution function which is an important quantity but this model remains expensive compared with usual fluid models. Therefore in this section we shall consider the Energy Transport model by assuming that the electrons are in local equilibrium and then the energy distribution function $F(x,\varepsilon)$ is a Maxwellian distribution

$$F(x,\varepsilon,t) = F(\varepsilon) = \exp\left(\frac{\mu(x,t)-\varepsilon}{T_e(x,t)}\right) \tag{3}$$

where $\mu \in \mathbb{R}$ and $T_e > 0$ are parameters respectively called the chemical potential and the temperature of the electrons, which depend on x and t.

As the phenomena (in particular secondary emission) take place essentially along the dielectric surface, we will consider a one dimension problem.

Therefore given the interpretation of $F(x,\varepsilon)$, for the maxwellian distribution $F(\varepsilon)$, we define the surfacic density n_e (m^{-2}) and the surfacic energy density We ($\mathrm{eV\,m}^{-2}$) of the electrons by

$$\begin{cases} n_e(x,t) = \int_0^{+\infty} F(\varepsilon)\,N(\varepsilon)\,d\varepsilon \\ W_e(x,t) = \int_0^{+\infty} F(\varepsilon)\,N(\varepsilon)\,\varepsilon d\varepsilon \end{cases} \tag{4}$$

where we recall that $N(\varepsilon)$ is the 'density of state'.

In the case of the Maxwellian (3) and of the linear potential profile (2) we have

$$n_e = C(T)\,e^{\mu/T_e}\ , \quad C(T) = C_0\frac{T_e^{5/2}}{E_T}\ , \quad C_0 = \left(\frac{2\pi q}{m_e}\right)^{3/2} \tag{5}$$

$$W_e = \frac{5}{2}n_eT_e$$

Integrating the diffusion model of (Ref. 6) with respect to ε, we find that $n_e(x,t)$ and $W_e(x,t)$ satisfy the following system

$$\frac{\partial}{\partial t}n_e + \nabla_x.j_n = q_n\ , \tag{6}$$

$$\frac{\partial}{\partial t}W_e + \nabla_x.j_w - j_n.\nabla_x\Phi_0 = q_w\ , \tag{7}$$

where

$$j_n = -D_{11}\left(\nabla_x\left(\frac{\mu}{T}\right) - \frac{\nabla_x\Phi_0}{T}\right) - D_{12}\nabla_x\left(-\frac{1}{T}\right)\ , \tag{8}$$

$$j_w = -D_{21}\left(\nabla_x\left(\frac{\mu}{T}\right) - \frac{\nabla_x\Phi_0}{T}\right) - D_{22}\nabla_x\left(-\frac{1}{T}\right)\ , \tag{9}$$

j_n and j_w being respectively the particle and energy currents; Φ_0 is the longitudinal potential along the surface where $E_0 = -\nabla_x\Phi_0$ is the electric field in the parallel direction to the dielectric side surface. The longitudinal potential Φ_0 is determinated by solving Poisson equation

$$-\Delta\Phi_0 = \frac{q}{d}\left(\frac{n_s}{\varepsilon_d} - \frac{n_e}{\varepsilon_0}\right) \tag{10}$$

where n_s is the positive surface charge accumulated by electron secondary emission, ε_d is the dielectric constant of the dielectric surface, ε_0 is the permittivity of free space and d is the layer of the electron plasma cloud. For the simulation we estimate this layer by the following quantity

$$d = \frac{T_e}{2\,|E_T|}. \tag{11}$$

q_n and q_w are terms of relaxation which takes account of the surface inelastic interactions and were be defined in the next section.

The diffusion matrix D is a symmetric 2×2 matrix

$$D = \begin{pmatrix} D_{11} & D_{12} \\ D_{21} & D_{22} \end{pmatrix} \tag{12}$$

and the coefficient D_{ij} are given by

$$\begin{aligned} D_{11} &= \tfrac{D_0}{|E_T|}n_eT_e^{3/2}\ , \\ D_{12} &= D_{21} = 4\tfrac{D_0}{|E_T|}n_eT_e^{5/2}\ , \\ D_{22} &= 20\tfrac{D_0}{|E_T|}n_eT_e^{7/2}\ , \\ D_0 &= 2\sqrt{\tfrac{2q}{m_e}} \end{aligned} \tag{13}$$

where m_e is the electron mass and q is the elementary charge

The particle and the energy currents (8)-(9) can be expressed in term of a mobility rate, therefore we have

$$\begin{aligned} j_e &= \mu_n\left[n_e.\nabla_x\Phi_0 - \nabla_x(n_eT_e)\right] + \alpha\nabla_xT_e \\ j_w &= \mu_w\left[n_e.\nabla_x\Phi_0 - \nabla_x(n_eT_e)\right] - \varkappa\nabla_xT_e \end{aligned} \tag{14}$$

where μ_n and μ_w are respectively the particle and the energy mobilities; α and $\varkappa$ are respectively the thermoelectric coefficient and the thermal conductivity.

In the case of the linear transverse potential profile (2), these parameters are given by

$$\mu_n = \tfrac{D_{11}}{n_eT_e}\quad , \quad \mu_w = \tfrac{D_{12}}{n_eT_e}\quad , \tag{15}$$

$$\begin{aligned} \alpha &= D_{11}\left(\frac{C(T_e)}{C'(T_e)} + \frac{1}{T_e}\right) - \frac{D_{12}}{T_e^2}\ , \\ \varkappa &= -D_{12}\left(\frac{C(T_e)}{C'(T_e)} + \frac{1}{T_e}\right) + \frac{D_{22}}{T_e^2}\ . \end{aligned}$$

A.2 The entropic structure of the energy-Transport system

It is more convenient to introduce the following variables

$$\varepsilon_F = \mu - \Phi_0 \quad ; \quad W_{e_T} = W_e - n_e\Phi_0 \quad ; \quad j_{w_T} = j_w - j_n\Phi_0 \tag{16}$$

where ε_F is the Fermi energy or electro-chemical potential, W_{e_T} is the total energy and j_{w_T} is the total energy current. Then the Energy-Transport model system (ref) can be written as

$$\frac{\partial}{\partial t}n_e + \nabla_x . j_n = q_n \ , \tag{17}$$

$$\frac{\partial}{\partial t}W_{e_T} + n_e\frac{\partial \Phi_0}{\partial t} + \nabla_x . j_{w_T} = q_w - q_n\Phi_0 \ , \tag{18}$$

with

$$j_n = -\widetilde{D}_{11}\left(\nabla_x\left(\frac{\varepsilon_F}{T}\right)\right) - \widetilde{D}_{12}\nabla_x\left(-\frac{1}{T}\right) \ , \tag{19}$$

$$j_w = -\widetilde{D}_{21}\left(\nabla_x\left(\frac{\varepsilon_F}{T}\right)\right) - \widetilde{D}_{22}\nabla_x\left(-\frac{1}{T}\right) \tag{20}$$

and

$$\begin{aligned} &\widetilde{D}_{11} = D_{11} \quad , \quad \widetilde{D}_{12} = \widetilde{D}_{21} = D_{12} - \Phi_0 D_{11} \quad , \\ &\widetilde{D}_{22} = D_{22} - 2\Phi_0 D_{12} + \Phi_0^2 D_{11} \ . \end{aligned} \tag{21}$$

III. Surfacic inelastic interaction

The electron surface interactions involve inelastic mechanisms such as attachment, secondary emission and desorption of adsorbed neutral. In addition the electrons can suffer collision with free neutral molecules present in the vacuum. In this section, we shall only discuss surface inelastic collisions and we neglect collisions with atoms and leave it for future work.

A. *Electron secondary emission*

In the energy transport system (17), (18), the two terms q_n and q_w are defined by

$$q_n = q_n^+ - q_n^- , \tag{22}$$

$$q_w = q_w^+ - q_w^- \ , \tag{23}$$

the loss terms (with a minus exponent) correponding to the attachment on the dielectric side surface and the gain term (with a plus exponent) correponding to a reemission.

The loss term can be written in the case of a linear transverse potential profile by

$$\begin{aligned} q_n^- &= \nu_0 . n_e \ , \\ q_w^- &= \tfrac{4}{5}\nu_0 . W_e \ , \end{aligned} \tag{24}$$

where ν_0 is a collision frequency with the dielectric side surface given by

$$\nu_0 = \sqrt{\frac{q}{2\pi m_e}}\frac{|E_T|}{T_e} \qquad \mathrm{s}^{-1} \tag{25}$$

The 'yield' γ_{ee} for the creation of secondary electrons is strongly dependent on the energy and angular distribution of the incident electrons. The following formula, given by (Ref. 4), for γ_{ee} is used

$$\gamma_{ee} = \gamma(\varepsilon,\theta) = \frac{\gamma_{\max}}{E_{\max}}\varepsilon_i \exp\left(2 - 2\sqrt{\frac{\varepsilon_i}{E_{\max}}}\right)\exp\left(2\left(1-\cos\left(\theta_i\right)\right)\right) \tag{26}$$

where ε_i is the incident energy, $E_{\max}$ is the incident energy for the maximum secondary electron yield, θ_i is the incident angle and $\gamma_{\max}$ is the maximum secondary yield at normal incidence.

We assume an isotropic distribution of the incident electronic particles and we define the mean yield (number of electrons reemitted for given incident energy ε_i) by

$$g\left(\varepsilon'\right) = \frac{\gamma_{\max}}{E_{\max}}\frac{\exp\left(2\right)}{2}\left(\exp\left(2\right) - 3\right)\varepsilon_i \exp\left(-2\sqrt{\frac{\varepsilon_i}{E_{\max}}}\right) \tag{27}$$

In order to define a physical model of secondary emission the following assumptions are made for one given incident electron :

- the incident electron is reemitted with 90% of its incident energy,
- secondary electrons are emitted and share uniformly the 10% remaining energy.

With these assumptions the gain term due to secondary emission are given by

$$\begin{aligned} q_n^+ &= \nu_n^+ . n_e \ , \\ q_w^+ &= \nu_w^+ . W_e \ , \end{aligned} \tag{28}$$

where

$$\begin{aligned} \nu_n^+ &= \nu_0 \int_0^{+\infty} u\exp(-u) g\left(T_e u\right) du \ , \\ \nu_w^+ &= \tfrac{\nu_0}{5}\int_0^{+\infty} u\exp(-u^2)\left(2-\chi\right) g\left(T_e u\right)\mathbf{1}_{[\mathbf{0},\mathbf{1}]}\left(\mathbf{g}\left(\mathbf{T_e u}\right)\right)\mathbf{du} \\ &\quad + \tfrac{2}{5}\nu_0 \int_0^{+\infty} u\exp(-u^2)\mathbf{1}_{[\mathbf{1},+\infty]}\left(\mathbf{g}\left(\mathbf{T_e u}\right)\right)\mathbf{du} \end{aligned} \tag{29}$$

and $\chi = 10\%$.

B. *Electronic stimulated desorption*

In this section, we are interested in the neutral density generated by Electron Stimulated Desorption. Indeed electron impact can give energy to the adsorbate and causes an electronic transition to the excited state of the adsorbate. In certain condition of the transition state, the adsorbated particles can leave the surface.

Following M.Cho (Ref. 4), we choose $\mathbf{H_2O}$ as the adsorbed species and we assume that, before the electron current begins to hit the surface, the adsorbed gas density is in a steady state.

We define by N_n^s and W_n^s respectively the surface density and the surface energy density of desorbed neutral, volumic density is then $N_n = \frac{N_n^s}{d_n}$ where d_n is the layer of the neutral cloud desorbed. We simply assume that the neutral cloud expands at the thermal velocity. This is given by

$$d_n = \int_0^t \sqrt{\frac{T_{surf}}{m_n}\left(x,s\right)}ds \tag{30}$$

where T_{surf} is the surface temperature and m_n is the neutral mass.

The surface desorption flux due to electronic impact is given by

$$\Gamma_{esd} = \frac{\partial n_n^s}{\partial t} = \nu_{esd}.n_e \tag{31}$$

where n_e is the incident electron surfacic density and ν_{esd} is the desorption frequency given by

$$\nu_{ESD} = \nu_0 . g_{maxD}\frac{T_e}{\varepsilon_T}\left[2 + \left(\frac{\varepsilon_T}{T_e} + 2\right).\exp\left(-\frac{\varepsilon_T}{T_e}\right)\right] \tag{32}$$

where

- $g_{maxD} = \sigma_{esd}.N_a$ is the maximum yield of the desorption

- $\varepsilon_T = \varepsilon_D . g_{maxD}$ (ε_D is the required desorption incident energy per neutral molecule)
- ν_0 is a collision frequency with the dielectric side surface given by (ref)
- T_e is the electron temperature (eV)

Since the surface neutral flux is proportional to the incident electron surface density, we can easily calculate the neutral density over the surface by the use of a numerical scheme (see section IV) with some assumptions about the surface adsorbed neutral density N_a and the desorption cross section σ_{esd}.

For simplicity, we assume a constant desorption cross section σ_{esd}. The adsorbed surface neutral density N_a is renewed continuously by substracting the number of neutral desorbed from its old value. Following M.Cho, the initial surface gas density (number of gas particles adsorbed per unit area) is assumed to be a monolayer $N_a = 10^{19}\ (\mathrm{m}^{-2})$ and the cross section is assumed to be $\sigma_{esd} = 5 \times 10^{-19}\ (\mathrm{m}^2)$. In this case the maximum yield $g_{maxD} = \sigma_{esd}.N_a$ is five gas molecules per one incident electron (and independent of the elctron incident energy if it is higher than 5 eV). The desorption yield of 5 molecules per electron corresponds to the maximum yield found in experimental studies (see Refs. 4, 5). The temperature of the desorbed gas is the same as the dielectric side surface assumed to be at $T_{surf} = 300\,(\mathrm{K})$. We assume that neutral molecules do not stick back to the surface.

C. *Enhanced field electron emission*

In (Ref. 4) the mechanism of electron emission is EFEE (enhanced field electron emission) and the electron current density emitted is given by

$$J = \frac{S_{FN}}{S_{\mathrm{real}}} A \left(\beta E_0\right)^2 \exp\left(-\frac{B}{\beta E_0}\right) \qquad \mathrm{A\,/\,m^2} \qquad (33)$$

which is the Fowler-Nordheim formula for field emission, with a field enhancement factor β. Here A and B are constants determined only by the work function ϕ_w of the conductor surface emission and E_0 is the electric field at the emission site. We assume that the electric field is enhanced by some mechanisms such as dielectric impurities or microscopic structures on the conductor surface (see Ref. 4 for details and references). Therefore S_{FN} is the area of the emission site on the conductor-dielectric interface and S_{real} is the area of the emission site on dielectric-vacuum interface (see figure 4)

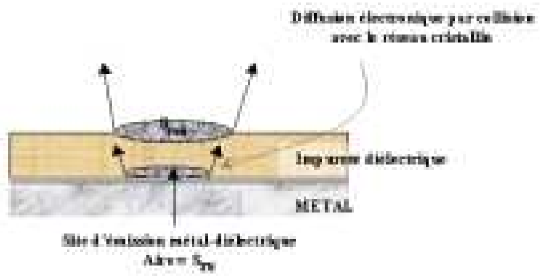

Figure 4 : EFEE site emission

IV. **Numerical schemes and results**

A numerical scheme was developed for a the one dimensional version of the energy transport system (17) - (18) with initial and boundaries conditions and for the Poisson equation. It consists in a finite volume method. For the time integration an implicit method was developed which allows us to use long time step without facing instability problems.

The model geometry consists in a $d = 0.1\,\mathrm{mm}$ thickness dielectric plate with $\varepsilon_d = 5,5\varepsilon_0$ (see figure 3) where $0.1\,\mathrm{mm}$ is a typical thickness of a solar cell coverglass and $\varepsilon_d = 5,5\varepsilon_0$ is a typical dielectric constant of dielectric plate like S_iO_2. The conductor is biased to $-700\ V$ while the dielectric front surface is biased to $0\ V$. For our geometry, it corresponds to an inverted potential gradient and the longitudinal electric field is initially 7×10^6 (V / m). We assume also an electric field of order 5×10^4 (V / m) perpendicular to the dielectric side surface leading to collisions of electrons emitted with the solid wall.

For the secondary emission we choose $\gamma_{\max} = 5,5$ and $E_{\max} = 500$ (eV) as typical value for S_iO_2.

For the field emitted electrons, we assumed cold emission, that is, the electrons are emitted with zero energy and $T_{efee} = 0$ (eV). A reasonable value for ϕ_w is $4,5$ eV as typical work function of a conductor.The constant A and B are given by

$$A = \frac{1.54\times10^{-10}\,10^{4.52/\sqrt{\phi_w}}}{\phi_w} \qquad \left(\mathrm{A\,/\,m^2}\right) \qquad (34)$$

$$B = 6.53 \times 10^9 \phi_w^{1.5} \qquad (\mathrm{V\,/\,m}) \qquad (35)$$

The emission site is located on the conductor and, following M.Cho (Ref. 4), we take $S_{FN} = 10^{-15}\ (\mathrm{m}^2)$ and $S_{\mathrm{real}} = 10^{-11}\ (\mathrm{m}^2)$.

Initially, we assumed that there is no plasma and no electrons confined along the dielectric surface. For the numerical resolution we choose the following initial conditions for the surface density and temperature of the electrons

$$n_e \mid_{t=0} \equiv 0.1\left(\mathrm{m}^{-2}\right) \qquad T_e \mid_{t=0} = 0.1\,(\mathrm{eV}) \qquad (36)$$

A. *Numerical results*

We show the time history of the electric field and the emission current density at the triple junction in figure 4 and figure 5.

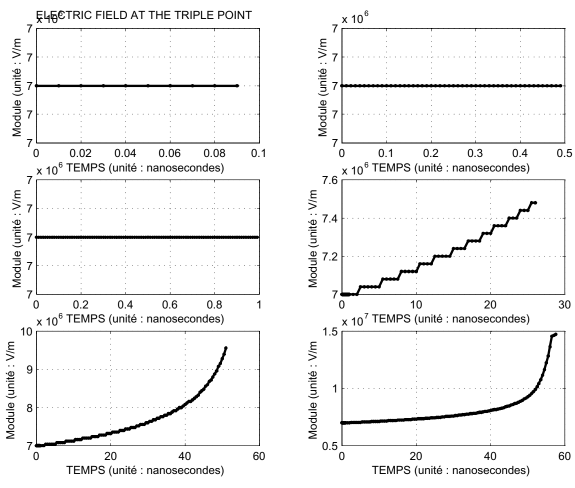

Figure 4 : Time history of electric field at the triple junction

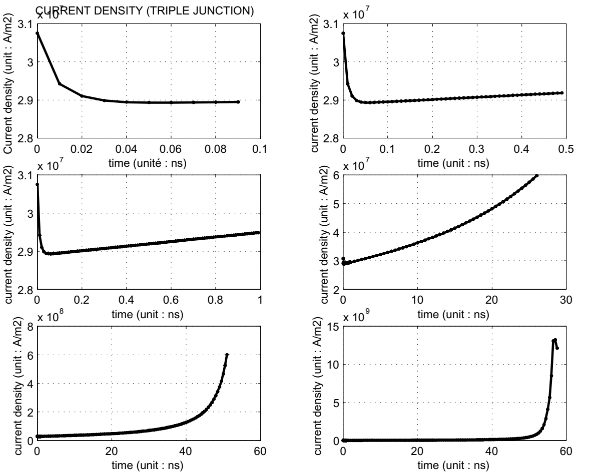

Figure 5 : Time history of the current density at the triple junctio

During 1 ns the electric field is in a steady state with an initial value $E_0 = 7 \times 10^6\,(\mathrm{V}\,/\,\mathrm{m})$; it increases rapidly after 5 ns to reache $1,6 \times 10^7\,(\mathrm{V}\,/\,\mathrm{m})$ of magnitude at t= 55 ns. The current density start decreasing because of the space charge effect produced by the emission current itself. As time goes on, the EFEE emission develops rapidly because of its exponential dependance on the field E_0. Starting with $3 \times 10^7\,\left(\mathrm{A}\,/\,\mathrm{m}^2\right)$, the current density at the triple junction is $1,5 \times 10^9\,\left(\mathrm{A}\,/\,\mathrm{m}^2\right)$ at t= 55 ns.

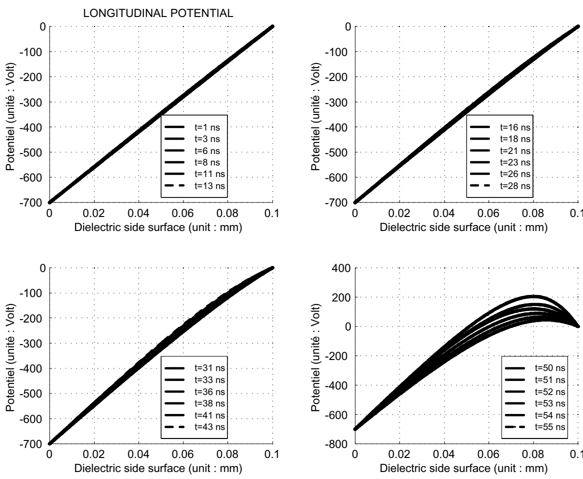

Figure 6 : Dielectric surface potential

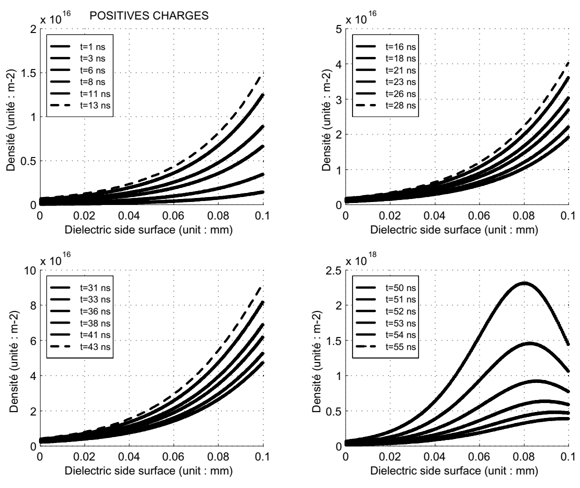

Figure 7 : Positive charges on the dielectric surface

We show the dielectric surface potential in figure 6 . As time goes on, the surface potential is more and more positive due to the increase of secondary electron emitted. The potential near the corner $x = d$ increases due to the fact that $\gamma_{ee} > 1$. Figure 7 shows the surface density of positive charges on the dielectric surface. One notes an accumulation of those at the end of the dielectric one. This is explained by the fact that the the place close to the anode ($x = 0.1\,\mathrm{mm}$) is the place where the electrons have high energy and it is on this level that the secondary emission is most intense.

In fact, the electrons emitted from the triple point, migrate towards the corner near $x = 0,1\,\mathrm{mm}$ while acquiring energy directed in the longitudinal electric field. This leads to a reinforcement of the transverse electric field as it is shown in Figure 8.

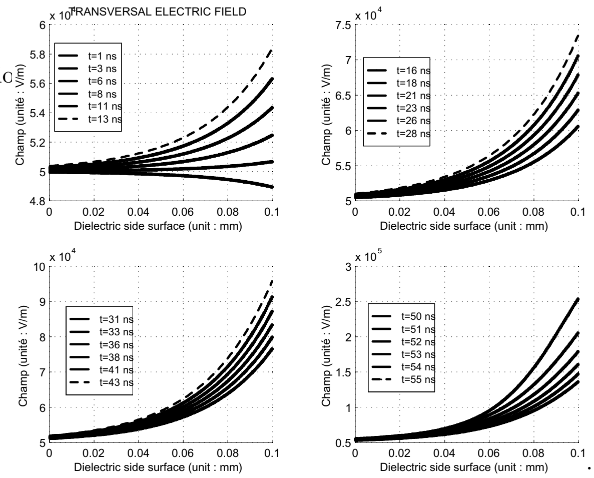

Figure 8 : Transverse electric field

Starting with 5×10^4 $(\mathrm{V}\,/\,\mathrm{m})$ of magnitude, it reaches to $2,5 \times 10^5$ $(\mathrm{V}\,/\,\mathrm{m})$ at the end of the simulation ($t = 55$ ns). The increase of the collision frequency at the dielectric wall results in a reinforcement of the secondary emission and the desorption.

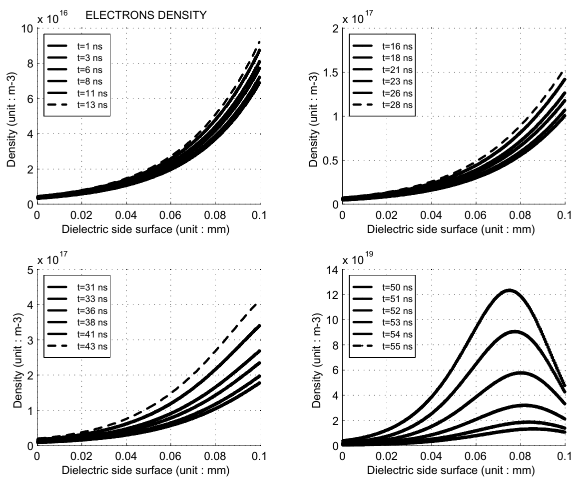

Figure 9 : Electrons density

Figure 9 shows the evolution of the density of the electrons confined along the dielectric wall. At $t = 1\,\mathrm{ns}$, the density of the electrons cloud is 7×10^{16} $\left(\mathrm{m}^{-3}\right)$ with a maximum near the corner $x = 0,1\,\mathrm{mm}$. The avalanche seems to occur after 50 ns. Figure 10 reveals a peak where the density reaches a value of $2,5 \times 10^{18}$ $\left(\mathrm{m}^{-3}\right)$. The density profile of neutrals is exactly identical to the one of electrons.Their density reaches a value of 5×10^{22} $\left(\mathrm{m}^{-3}\right)$ at the end of the simulation.

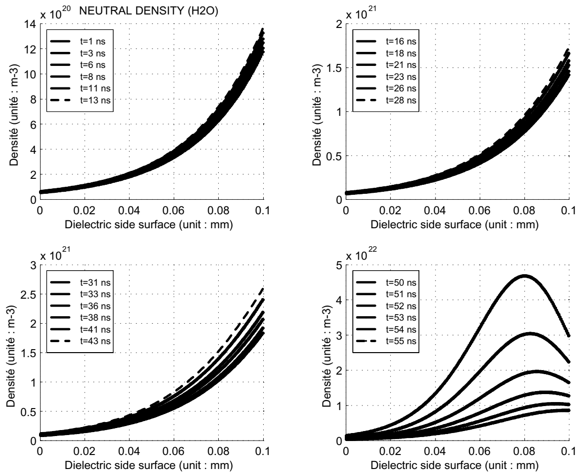

Figure 10 : Neutral density (H_2O)

V. Conclusion

In this work, we have established a fluid model, more convenient for numerical simulation, for the study of dielectric discharges. An analysis of the primary discharge was developed on the idea of the discharge being driven by electric fied runaway time at the triple junction, secondary emission and finally neutral desorption. The numerical simulation gives us qualitative results and shows clearly that the secondary emission play a role in the formation of a plasma cloud.

Future work will include collisions with neutral molecules in order to evaluate the probably apparition of ions.

References

[1] N. BEN ABDALLAH, P. DEGOND, 1996, On a hierarchy of macroscopic models for semiconductors, *J.Maths.Physics*. **37**, 3306-3333.

[2] P. DEGOND, R. TALAALOUT, M.H. VIGNAL, June 2000, Modélisation d'Arcs sur les Panneaux Solaires Opérant à Tension Elevée, EMAGS Technical, *Laboratoire M.I.P*

[3] W. S. BOYLE, P. KISLIUK, L. H. GERMER, 1955, Electrical Breakdown in High Vacuum, *J. of Appl. Phys.*, **26**, 720-725.

[4] M. CHO, 1992, Arcing on High Voltage Solar Arrays in Low Earth Orbit: Theory and Computer Particle Simulation, *Phd thesis, Massachusetts Institute of Technology*

[5] M. CHO, D.E HASTINGS., 1990, Dielectric Charging Process and Arcing Rates of High Voltage Solar Arrays, *J. Spacecraft and Rockets*, **28**, 698-706.

[6] P. DEGOND, 1999, Transport of trapped particles in a surface potential, *préprint*

[7] P. DEGOND, B. LUCQUIN-DESREUX, 1996, Transport coefficient of plasma and disparate mass binary gases, *Transport Theory and statistical Physics*, **25**, 595-633.

[8] P. DEGOND, C. SCHMEISER, 1999, Kinetic boundary layers and fluid -kinetic coupling in semiconductors, *Transport Theory and statistical Physics*, **28**, 31-55.

[9] D. E. HASTINGS, M. CHO, H. KUNINAKA, 1992, Arcing Rates for High Voltage Solar Arrays: Theory, Experiment, and Predictions, *J. Spacecraft and Rockets*, **4**, 538-554.

[10] D. E. HASTINGS, G. WEYL, D. KAUFMAN., 1990, Threshold Voltage for Arcing on Negatively Biased Solar Arrays, *J. Spacecraft and Rockets*, **27**, 539-544.

[11] I. KATZ, D. B. SNYDER., 1998, Mechanism for Spacecraft Charging Initiated Destruction of Solar Arrays in GEO, *AIAA 98-1002, 36th Aerospace Sciences Meeting & Exhibit*, *RENO, NV*

[12] D. E. PARKS, G. A. JONGEWARD, I. KATZ, V. A. DAVIS, 1987, Threshold-Determining Mechanisms for Discharges in High-Voltage Solar Arrays, *J. Spacecraft and Rockets*, **24** , 367-371.

[13] J. D. SOLDI, D. E. HASTINGS, D. HARDY, D. GUIDICE, K. RAY, 1997, Flight Data Analysis for the Photovoltaic Array space Power Plus Diagnostics Experiment, J. Spacecraft and Rockets, **34**, 92-103.

[14] G.E VIBRANS, 1964, Field Emission in Vacuum Voltage Breakdown, *Technical Report 353, Lincoln Lab, M.I.T*